Supplemental material for: "Evidence for long-lived quasiparticles trapped in superconducting point contacts"

M. Zgirski[1], L. Bretheau, Q. Le Masne, H. Pothier, D. Esteve and C. Urbina
Quantronics Group, Service de Physique de l'État Condensé (CNRS, URA 2464), IRAMIS, CEA-Saclay, 91191 Gif-sur-Yvette, France
(Dated: May 24, 2011)

We first discuss the various representations of the spectrum of Andreev bound states, then the sample design and fabrication, and the switching current measurements. The details of the poisoning dynamics measurements are then reported, followed by a description of a procedure, nicknamed "poisoning antidote", to untrap quasiparticles from the point contact. A discussion of the various processes at play follows, with a presentation of the results in terms of poisoning and unpoisoning rates as a function of the energy of the Andreev states. Details on the dynamics of our circuit are discussed in appendix A. Appendix B focuses on the calculation of the relaxation rate from the spin-singlet double excitation.

PACS numbers:

I. ANDREEV BOUND STATES REPRESENTATIONS

The widely used picture for Andreev bound states (ABS) in a short single channel conductor is the semiconductor representation[2,3] shown in Fig. 1, assuming spin degeneracy (continuum states at energies smaller than $-\Delta$ and larger than Δ are not shown). The lines correspond to the energies of the available energy levels. In the ground state, all levels at negative energies are occupied. The total energy has a single phase-dependent term $-E_A(\delta)$, arising from the lowest ABS. When adding a single quasiparticle to the system (quasihole or quasielectron), one accesses the two odd configurations, which correspond to the ABS being both empty or both occupied. Both configurations have zero energy ($-E_A$+E_A or 0+0), in absence of magnetic field or spin-orbit coupling[4,5]. Finally, adding two quasiparticles or exciting the system with photons at energy $2E_A$ gives access to the spin-singlet double-excitation configuration, represented here with the lowest ABS being empty and the top one being occupied. The excitation spectrum shown in Fig. 1d of the Letter directly follows: at a given phase δ, two possible single particle excitations have an energy E_A above the ground state energy; the cost of the double excitation is $2E_A$.

An alternative representation, used in Ref. 5 shows the energy of the various configurations as a function of the phase difference. Without spin-dependent interactions, one obtains Fig. 2.

As discussed in the main paper, the vanishing of the supercurrent is interpreted as arising from poisoning of the Andreev doublet by a single quasiparticle, *i.e.* a transition from the ground state$|0\rangle$ to an odd configuration $|1\uparrow\rangle$ or $|1\downarrow\rangle$. We think that the following description, although not rigorous, helps clarifying the nature of the Andreev states and their spin structure: in the ground state of the system, a Cooper pair state (spin singlet state) is formed at the contact with an energy $-E_A(\delta) \in [-\Delta, 0]$, through Andreev reflections in the superconductors on both sides. Mimicking the BCS theory in second quantization formalism[2], and inspired by Ref. [6,7], the superconducting ground state wave-function at the contact can be thought of as

$$|\Psi_0\rangle = |\Psi_{cont}\rangle \otimes \left(u_A + v_A c^\dagger_{A\uparrow} c^\dagger_{A\downarrow}\right)|0\rangle\,, \qquad (1)$$

with $|\Psi_{cont}\rangle$ describing the states with energy lying below $-\Delta$ (continuum states) and $|0\rangle$ is the vacuum. We have singled-out from the BCS wave-function the state "A" corresponding to the lowest energy Andreev state. The creation operators $c^\dagger_{A\uparrow,\downarrow}$ create an electron at the Fermi level in the channel, with either spin. Hence, the coefficients u_A and v_A differ only by a phase, and

$$|\Psi_0\rangle = |\Psi_{cont}\rangle \otimes \frac{1}{\sqrt{2}}\left(1 + e^{i\delta_A} c^\dagger_{A\uparrow} c^\dagger_{A\downarrow}\right)|0\rangle\,. \qquad (2)$$

Thus, the Andreev energy $-E_A$ can be seen as the condensation energy of the "Andreev Cooper pair".

The addition of one quasiparticle to the system at the lowest possible energy is described by one of the two Bogoliubov operators $\gamma^\dagger_{A\uparrow} = u^*_A c^\dagger_{A\uparrow} - v^*_A c_{A\downarrow}$ or

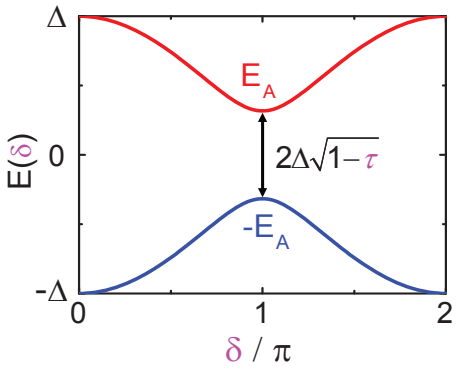

Figure 1: Phase (δ) dependence of the Andreev bound states energies $\pm E_A$ in a short transport channel of transmission τ. The energy Δ is the superconducting gap.

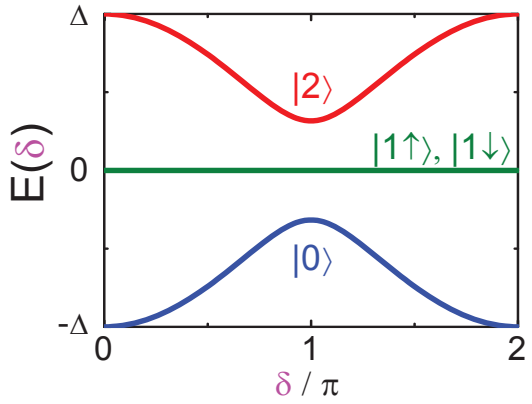

Figure 2: Energy of the different configurations accessible to a single channel. The energy of the ground configuration, labeled $|0\rangle$, is that of the lowest Andreev level $-E_A$ of Fig. 1. Two odd configurations, labeled $|1\uparrow\rangle$ and $|1\downarrow\rangle$, with one quasiparticle added to the ground state, have zero energy and a definite spin[5]. In the configuration $|2\rangle$, only the excited Andreev state $+E_A$ is occupied.

$\gamma^\dagger_{A\downarrow} = u^*_A c^\dagger_{A\downarrow} + v^*_A c_{A\uparrow}$, which lead to the "odd" states

$$|\Psi_{1\uparrow}\rangle = \gamma^\dagger_{A\uparrow}|\Psi_0\rangle = |\Psi_{cont}\rangle \otimes c^\dagger_{A\uparrow}|0\rangle \tag{3}$$

and

$$|\Psi_{1\downarrow}\rangle = \gamma^\dagger_{A\downarrow}|\Psi_0\rangle = |\Psi_{cont}\rangle \otimes c^\dagger_{A\downarrow}|0\rangle\,, \tag{4}$$

both having a single electron occupying with certainty the state at the Fermi energy. The energy of the odd states is higher than the ground state energy by the condensation energy E_A of the Cooper pair in the Andreev bound state. For completion, the upper Andreev state $|\Psi_2\rangle$ is obtained when two quasiparticles are added to the ground state, at an energy cost $2E_A$:

$$\begin{aligned}|\Psi_2\rangle &= \gamma^\dagger_{A\downarrow}\gamma^\dagger_{A\uparrow}|\Psi_0\rangle = -\gamma^\dagger_{A\uparrow}\gamma^\dagger_{A\downarrow}|\Psi_0\rangle \\ &= |\Psi_{cont}\rangle \otimes \left(u^*_A c^\dagger_{A\uparrow}c^\dagger_{A\downarrow} - v^*_A\right)|0\rangle\,.\end{aligned} \tag{5}$$

Apart from a non-physical global phase, this state can be rewritten as $|\Psi_{cont}\rangle \otimes \frac{1}{\sqrt{2}}\left(-1 + e^{i\delta_A}c^\dagger_{A\uparrow}c^\dagger_{A\downarrow}\right)|0\rangle$, which resembles the ground state $|\Psi_0\rangle$: it contains an excited Cooper pair (excited singlet). As a matter of fact, the present experiment was initially designed to perform the spectroscopy of the transition between $|\Psi_0\rangle$ and $|\Psi_2\rangle$, a goal that we haven't reached yet.

II. SAMPLE FABRICATION AND MEASUREMENT SETUP

The samples were fabricated on a polished, 500 µm-thick Kapton substrate, which is insulating and elastic. A suspended bridge is fabricated by e-beam lithography of a thin constriction in an aluminum film, and etching of 1 µm of an underlying polyimide layer. Optical micrographs of the sample at various scales, a SEM micrograph of the core of the sample and a photograph of the break-junction mount used to obtain atomic contacts are shown in Fig. 3. The bridge is placed in a superconducting loop containing also a 2.8 µm^2 Josephson junction fabricated at the same time by shadow evaporation (70 nm Al, oxidation in an $Ar - O_2$ (85%-15%) mixture at 18 mbar for 5 min, 54 nm Al), hence forming a SQUID[8,9]. The SQUID is connected with thin (124 nm), narrow (0.9 µm) and long (0.4 and 0.8 mm) Al wires corresponding to a total inductance L in the nH range. At a larger scale, the connecting wires overlap over 0.01 mm^2 a floating underlying 30 nm-thick aluminum electrode, which was covered with five heavily oxidized 1.5 nm-thick aluminum layers, forming a capacitor $C \simeq 65$ pF, hence shunting the connecting lines at high frequency. The resonance frequency $(2\pi\sqrt{LC})^{-1} \simeq 0.5$ GHz and the losses of the corresponding tank circuit (see Fig. 4), modelled by series resistance $r \simeq 0.5\,\Omega$, were measured by microwave reflectometry in a separate experiment with the same sample. From the capacitor, a 50 Ω coplanar waveguide makes the connection towards a mm-size connection pad placed at the edge of the sample.

The sample was cooled in a dilution refrigerator operated down to 25 mK. The substrate is clamped at one of its edges, between a small copper plate placed underneath and the half-cylindrical central pins of two SMA launchers, which connect to the bias and fast flux lines[11] (see Fig. 3(e)). Connections of the ground plane to the sample holder are achieved in the same manner[12]. The atomic contacts are obtained by bending the sample with a pusher placed on the side opposite to the contact pads. The contacts formed with this setup are very stable. For example, the contact discussed in the Letter, labeled AC1 in the following, was kept unchanged during 2 months, till we decided to form another one. A shielded superconducting coil (which had been withdrawn before taking the picture in Fig. 3(e)) is placed a mm above the SQUID, for dc flux biasing. Bias lines connected to the SQUID and to the antenna are coaxial lines heavily attenuated at various stages of the cryostat, with total attenuation of 55 and 30dB, respectively, in order to damp the current noise of the components placed at higher temperature. The current and voltage measurement lines are twisted pairs, equipped with micro-fabricated microwave filters[13].

III. DETERMINATION OF THE TRANSMISSION COEFFICIENTS

The current-voltage characteristic of the Josephson junction alone, taken after opening completely the atomic contact, is shown with black open symbols in Fig. 5. As observed in other experiments with similar junctions[9,11,14], some current is found at sub-gap voltages, here for $|V| < 200\,\mu$eV. The large scale resistance

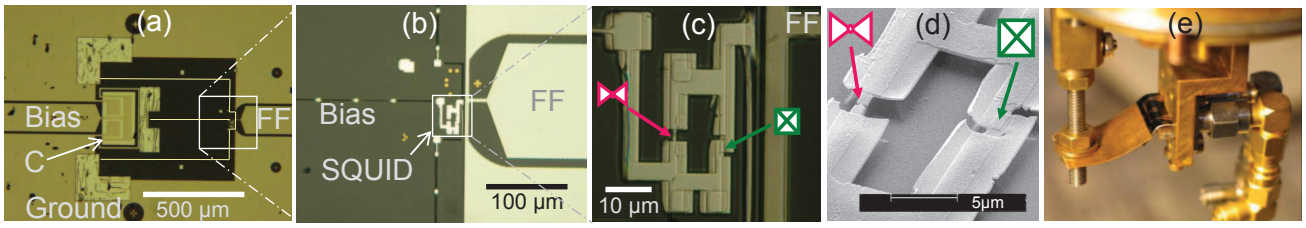

Figure 3: (a) Large scale photograph of the sample, showing the end of the fast flux (FF) and current bias coplanar lines. The bias line and the ground plane form planar capacitors with a common, floating and superconducting rectangular electrode placed below, implementing the capacitor C. From there the connections to the SQUID are made with 0.9 µm-wide Al wires which are not visible at this scale, and have been redrawn for clarity. They appear on the photograph (b) as three dark lines with regularly spaced bright spots, one connected to the bias line, the two others to the ground plane. The bright spots are wider pillars that hold on the substrate since they are large enough not to be completely freed during the etching step. The fast flux coplanar line ends with a short close to the SQUID, the current in the upper half of the short creating a magnetic flux in the loop. Photograph (c) shows the SQUID loop, with the Josephson junction on the right and the suspended bridge where the atomic contacts are formed on the left. Five small square gold electrodes, intended as quasiparticle traps[10], are barely visible through the Aluminum layers. (d) SEM micrograph of the SQUID, seen under an angle: two angle evaporation of aluminum define the superconducting loop with a tunnel junction on the right arm, and a suspended micro-bridge on the left arm, which is broken at low temperature to form atomic contacts. (e) View of the sample holder, with a bent sample. The sample is clamped between the launchers of two SMA connectors, which are visible on the right-hand side, and a small metallic plate hold with two screws at the bottom. The sample is bent with a brass blade held by a rod moving vertically (on the left). For this photograph, the bending was exagerated, and the superconducting coil placed immediately above the sample was removed.

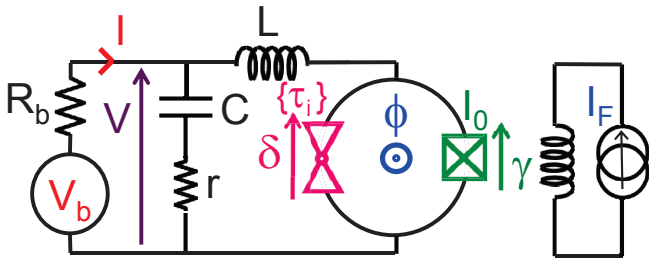

Figure 4: Full schematic of the sample. The SQUID is biased through an on-chip LC circuit ($L \simeq 1.6\,\mathrm{nH}$, $C \simeq 65\,\mathrm{pF}$). The losses in the capacitor are modelled by series resistance $r \simeq 0.5\,\Omega$. The voltage V measured across the full on-chip circuit corresponds, at low frequency, to the voltage drop across the SQUID.

is $R_{JJ} = 550\,\Omega$. The same figure presents with red solid symbols the $I-V$ characteristic of a SQUID with an atomic contact: as compared to the previous curve, the large scale conductance is slightly increased, and a significant sub-gap current is visible. The difference between the two characteristics, which represents the contribution of the atomic contact to the dissipative current, is shown in the inset with green open symbols. It is fitted with the theory[15–17] of Multiple Andreev Reflections (MAR)[18] in order to obtain the transmission of its conduction channels[19]. The region $|V| < 200\,\mu\mathrm{eV}$, where sub-gap current was already found in the $I-V$ characteristic of the Josephson junction by itself, was excluded from the fit. As a consequence, the accuracy on the determination of the transmissions of the channels is not as good as in experiments with atomic contacts alone[20]. It is here of the order of 1% for the largest transmission, and 3% for the second largest. As an example, the contact corresponding to Fig. 5, called AC0 in the following, was found to have 3 channels, as most one-atom Aluminum contacts do; their transmissions, deduced from the fit of the $I-V$ characteristic, are $\{0.95,0.45,0.10\}$. The corresponding fit is shown in the inset of Fig. 5 as a solid line.

IV. SWITCHING CURRENT MEASUREMENTS

The supercurrent associated with the phase-dependence of the Andreev bound states energy is accessed through measurements of the "switching current" of the SQUID (see Fig. 5). The geometrical inductance of the loop, of the order of 20 pH[11], can be neglected when compared to the Josephson inductances of the junction ($L_{JJ} = \varphi_0/I_0 \simeq 0.6\,\mathrm{nH}$) and of the atomic contact ($L_{AC} \sim 4\varphi_0^2/\tau\triangle \simeq 10\,\mathrm{nH}$). Therefore, the phase γ across the Josephson junction, the phase δ across the atomic contact and the flux phase $\varphi = 2\pi\phi/\phi_0$ are related through $\varphi = \delta - \gamma$.

The modulation of the switching current of the SQUID

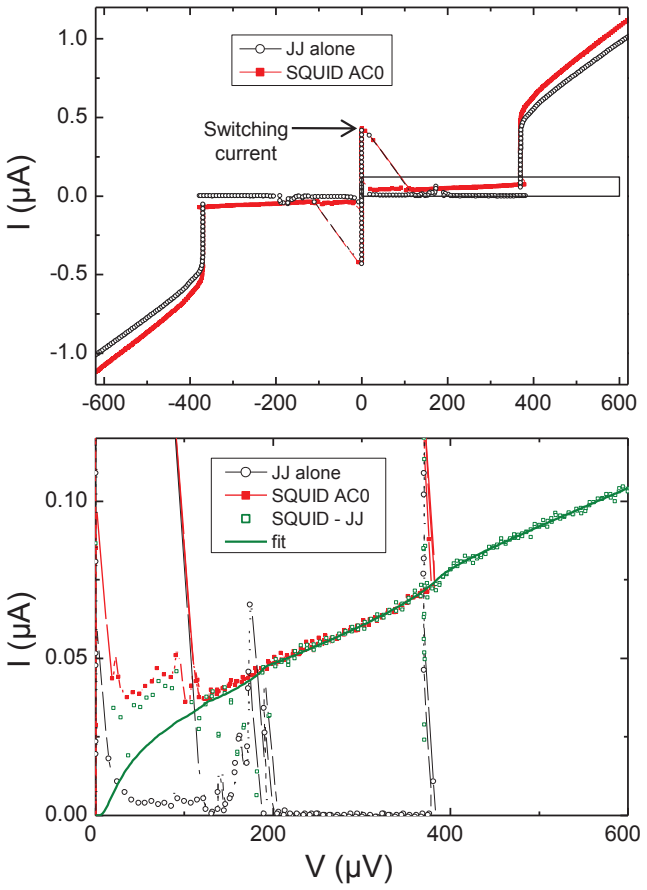

Figure 5: Top: Current-voltage ($I-V$) characteristics of the Josephson junction (black open symbols) and of a SQUID with an atomic contact labeled AC0 (red filled symbols). The switching current of the SQUID, indicated with an arrow, is modulated by the applied flux. Bottom: same data, and (green open symbols) $I-V$ characteristic of the atomic contact alone obtained by subtraction of the one of the junction from that of the SQUID. The transmissions $\{0.95,0.45,0.10\}$ are found by fitting this $I-V$ characteristic with the theory of Multiple Andreev Reflexions (green solid curve), excluding the region $|V|<200\,\mu$eV where the $I-V$ characteristic of the Josephson junction presents resonances.

can be qualitatively understood as follows[11]: when a flux is applied, the flux phase φ drops mainly across the weakest link in the loop, *i.e.* the atomic contact. In contrast, when a bias current I is applied, it flows essentially in the arm with the largest critical current, which is the one with the Josephson junction. As a consequence, $\gamma \simeq \gamma(s) \equiv \arcsin(s)$ and $\delta \approx \varphi+\gamma(s)$, with $s=I/I_0$ the normalized current and I_0 the critical current of the Josephson junction alone. The current circulating in the SQUID loop, which is due to the phase-biased atomic contact, is therefore $I_{at.c.}(\varphi+\gamma(s)) = \sum_i c_i I_A(\varphi+\gamma(s),\tau_i)$, and the total current through the Josephson junction $I-I_{at.c.}(\varphi+\gamma(s))$. Since $I_A \ll I_0$, the switching current of the SQUID will be close to the switching current $I_{sw}^{JJ} = s_{sw}^{JJ} I_0$ of the junction alone, and $\gamma(s) \simeq \gamma\left(s_{sw}^{JJ}\right)$.

In the experiments presented here, switching for the junction alone occurs around $s_{sw}^{JJ} \approx 0.88$, and $\gamma\left(s_{sw}^{JJ}\right) \approx 0.3\pi$. As a consequence, switching for the SQUID occurs when $I - I_{at.c.}\left(\varphi+\gamma(s_{sw}^{JJ})\right) \approx I_{sw}^{JJ}$: the average switching current is that of the junction alone, and the modulation corresponds, in a first approximation, to the current-phase relation of the atomic contact, with a phase offset. The modulation of the switching current by the flux is therefore a direct measurement of the current-phase relation of the atomic contact and not, as one could believe at first sight, a measure of the *switching* current of the atomic contact alone.

Initially we performed switching measurement using a standard pulse technique: a train of current pulses of normalized height $s=I/I_0$ is applied through the bias line, while monitoring the voltage across the SQUID to reveal switching. The total number of voltage pulses for a given current pulse train is recorded with a counter, see Fig. 6. In order to have detectable voltage pulses even if

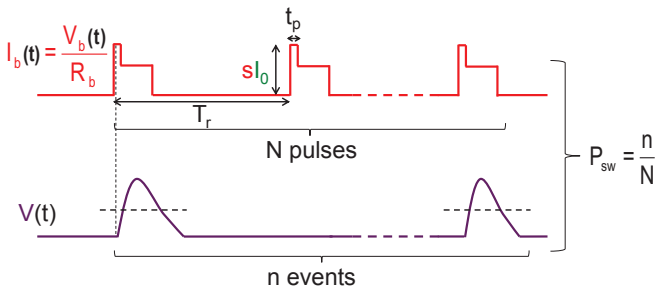

Figure 6: Standard switching probability measurement scheme: a train of N pulses with normalized height sI_0 and duration t_p are applied on the bias of the SQUID. The repetition rate is $1/T_r$. The 40% lower plateau following each pulse holds the voltage at a finite value if switching has occurred, hence facilitating detection. The number n of voltage pulses resulting from switching events is recorded by a counter detecting crossings through a threshold value (dotted line). The switching probability is then $P_{sw} = \frac{n}{N}$.

switching occurs at the end of the bias pulse, the actual bias pulse is followed by a 40% lower plateau that "holds" the voltage at a finite value for a time long enough for it to be detected. The height of this plateau is such that the switching probability during its duration is negligible. We used a bias pulse duration t_p =1 μs, and 5 μs-long "hold" plateaus. In general, the repetition period T_r was 20 μs. The switching probability $P_{sw}(s)$ is obtained as the ratio of the number of measured voltage pulses to the number of bias pulses (typically 10^4). The inset of Fig. 7 shows the resulting switching probability P_{sw} as a function of the normalized pulse height s, for two values of the flux phase corresponding to switching currents close to its maximum and minimum values: $\varphi_1 = 0.20\pi$ (black symbols) and $\varphi_2 = 0.97\pi$ (orange symbols). Whereas the shape of the former (at φ_1) corresponds to what is usually found on Josephson junctions, with a sharp variation of the probability from 0 to 1 as the pulse height is increased, the latter (at φ_2) presents an unusual long

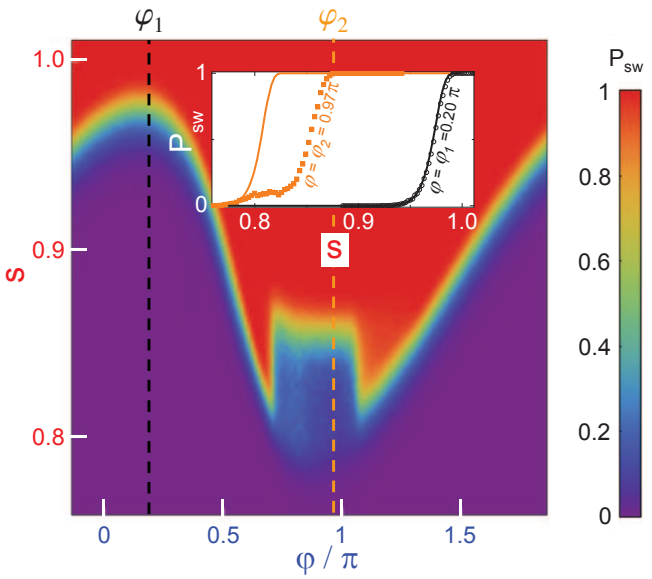

Figure 7: Switching probability P_{sw} measured using the standard method (see Fig. 6) as a function of flux phase φ and of the normalized pulse height s for the SQUID with contact AC0 ($\{0.95,0.45,0.10\}$). Inset: $P_{sw}(s)$ for fluxes $\varphi_1 = 0.20\pi$ (black, open symbols) and $\varphi_2 = 0.97\pi$ (orange, full symbols). Solid curves correspond to theoretical predictions.

foot. The two types of behaviors are seen in the main panel of Fig. 7, a color plot of P_{sw} with φ and s on the axes. Whereas the transition from $P_{sw} \simeq 0$ (purple) to $P_{sw} \simeq 1$ (red) is abrupt for most values of φ, an anomalous region with an almost constant intermediate step at $P_{sw} \simeq 0.1$ (blue) is observed for $0.7\pi < \varphi < 1.1\pi$. In this region, the analysis of the histogram of time delays between switching events shows that they are correlated, with bunches of switching events and long "blind" periods without any switching. This behavior is reminiscent of the "blinking" observed in the fluorescence of molecules or quantum dots[21,22].

Correlations disappear when a strong bias pulse that forces the system to switch (pulse height 30% higher that the measurement pulse, see Fig. 8) is applied before each measurement pulse (of course, the corresponding forced switching events are ignored in the counting). During the prepulses, a voltage develops across the atomic contact, and both the energy and the occupation of the Andreev levels evolve at the Josephson frequency. When the current is reset to zero, the Andreev levels are back to their energies $\pm E_A(\delta, \tau_i)$, but the system is left in an out-of-equilibrium situation, which on average is always the same. The measurement pulse is applied a time Δt after this reset. Using such "switching prepulses", the switching probability is independent of T_r, and the histograms of time intervals between switching events do correspond to independent processes. As reported in the main text, the corresponding curves $P_{sw}(s)$ then display a well defined intermediate plateau, as seen for flux φ_2 in the inset of Fig. 9.

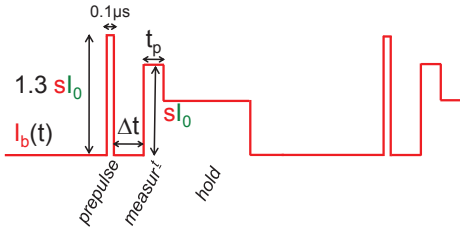

Figure 8: Measurement scheme used in the following and for the data shown in the Letter. Short prepulses 30% higher than the actual measurement pulses cause the system to always switch. With such pulses, successive switching events are uncorrelated.

V. CALCULATION OF SWITCHING PROBABILITY

We now give the details of the theoretical model used in the main paper to describe the switching probability $P_{sw}(s, \varphi)$. It is related to the switching rate $\Gamma(s, \varphi)$ and to the pulse duration t_p by $P_{sw} = 1 - \exp(-\Gamma t_p)$. The phase γ across the Josephson junction is a dynamical variable governed by a Langevin equation, equivalent to the one obeyed by the position of a massive particle evolving in a "tilted washboard potential"[23–25]. The total potential of the SQUID is given by[9]:

$$U(\gamma) = -E_J \cos\gamma - E_J s\gamma + \sum_i c_i E_A(\gamma + \varphi, \tau_i) \qquad (6)$$

where the first term is the Josephson energy of the tunnel junction, with $E_J = I_0\varphi_0$, the second one is the energy arising from the coupling to the bias source, and the last term is the total Josephson coupling introduced by the atomic contact, which depends on the configuration of the Andreev levels ($c_i = -1$ if channel i is in its ground state, $c_i = 1$ in excited singlet, and $c_i = 0$ in an odd configuration). Since $E_J/\Delta \simeq 5.7 \gg 1$, the two first terms in Eq. (6) dominate, and the shape of the tilted potential resembles that of a single Josephson junction, with slightly modified barrier height $\Delta U(s, \varphi)$ and plasma frequency $\omega_p(s, \varphi)$. As in Ref. 9, switching can be fitted with thermal escape theory[26], with a rate $\Gamma = A\exp(-B)$ with $B = \Delta U/k_BT$ and $A \simeq \omega_p/2\pi$. When the atomic contact is open, the plasma frequency in the tilted potential is $\omega_p = \omega_0(1-s^2)^{1/4}$, with $\omega_0 \approx \sqrt{I_0/\varphi_0 C_{JJ}}$, $C_{JJ} = 0.21\,\mathrm{pF}$ the Josephson junction capacitance estimated from its area[11], and $\Delta U \simeq (4\sqrt{2}/3)E_J(1-s)^{3/2}$ the barrier height[27]. Fitting $P_{sw}(s)$ for the Josephson junction alone gives $I_0 = 553.7\,\mathrm{nA}$ ($\omega_0/2\pi \approx 15\,\mathrm{GHz}$), and an effective temperature $T = 100\,\mathrm{mK}$[28]. When an atomic contact is formed, precise comparison between experiment and theory is performed using a numerical determination of the barrier height, and of the plasma frequency $\omega_p(s, \varphi)$ from the semi-classical calculation of the energy levels in the actual potential. More details on the SQUID potential are given in Appendix A.

The predictions for the $P_{sw}(s)$ curves of the SQUID

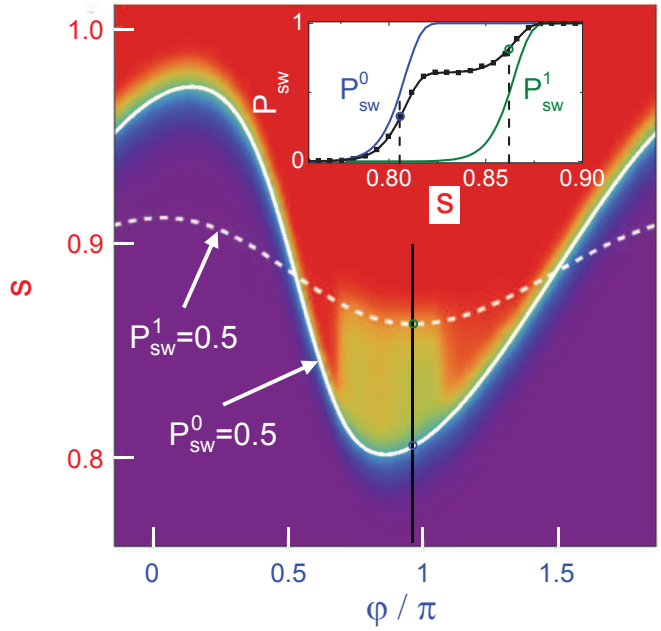

Figure 9: Color plot of the switching probability $P_{sw}(s,\varphi)$ using switching prepulses (see Fig. 8, $\Delta t = 0.5\,\mu$s) for the SQUID with contact AC0 with transmissions {0.95,0.45,0.10}. The color scale is the same as for Fig. 7. The white curves show the lines corresponding theoretically to $P_{sw} = 0.5$ for the pristine contact ({0.95,0.45,0.10}, solid line) and for the contact with the first channel poisoned (dashed line). Inset: cut at $\varphi = 0.97\pi$ (black line in the main panel). Black symbols: $P_{sw}(s)$ as measured; solid curves: theoretical curves, $P^0_{sw}(s)$ (leftmost, blue online) for the pristine contact ({0.95,0.45,0.10}) and $P^1_{sw}(s)$ (rightmost, green online) for the poisoned contact, i.e. without the contribution of the most transmitting channel; intermediate line (black): fit of the data with the linear combination given by Eq. (7) with $p = 0.36$.

with contact AC0 are shown as solid lines in the insets of Figs. 7 and 9. Whereas the curve taken at $\varphi = \varphi_1 = 0.20\pi$ in Fig. 7 is well fitted by theory, the curve taken at $\varphi = \varphi_2 = 0.97\pi$ has in common with theory only the value of s where the switching probability starts to rise. A central point of the paper is that, when prepulses are used (Figs. 9), the curve with a plateau can be very precisely accounted for by the weighted sum of two $P_{sw}(s)$ curves corresponding to two different configurations of the contact, as shown in the inset of Fig. 9: $P_{sw}(s) = (1-p)P^0_{sw}(s) + pP^1_{sw}(s)$, with $p = 0.36$, as well as in the inset of Fig. 2 in the Letter. The first one, $P^0_{sw}(s)$, is the one predicted for the pristine contact; the second one, $P^1_{sw}(s)$, is that of the poisoned contact, *i.e.* with its most transmitting channel in an odd configuration. This is the case in the whole flux region where the switching curves have an intermediate plateau, as shown in the main panel of Fig. 9. As in the Fig. 2 of the Letter, we compare the data with the two lines corresponding to the equations $P^{0,1}_{sw}(s,\varphi) = 0.5$. In the regions where $P_{sw}(s)$ has a standard shape, $P_{sw}(s)$=0.5 occurs at the position predicted for the pristine contact ($P^0_{sw}(s)$). In the region $0.7\pi < \varphi < 1.1\pi$, $P_{sw}(s)$ has two steps (which appear in the figure as color gradients): one occurs at the position where $P^0_{sw}(s,\varphi) = 0.5$ (solid line), the other one at the position where $P^1_{sw}(s,\varphi) = 0.5$ (dashed line), showing that

$$P_{sw}(s,\varphi) = (1-p(\varphi))P^0_{sw}(s,\varphi) + p(\varphi)\,P^1_{sw}(s,\varphi)\,. \quad (7)$$

In Fig. 10, similar comparisons are presented for three other SQUIDs formed with atomic contacts having one channel almost perfectly transmitting and the other ones with transmissions lower than 0.7. There again, in a broad phase range around π, $P_{sw}(s)$ shows a plateau delimited by the predictions for the pristine (solid line) and for the poisoned configurations, i.e. with the more transmitting contact in an odd configuration (dashed line).

VI. MEASUREMENTS OF POISONING DYNAMICS

A. Method

The previous experiments demonstrate that, in a certain parameter region, the system has a finite probability p to trap a quasiparticle and end in an odd configuration after the prepulse. In the following, we describe the experiments exploring the dynamics of trapping and untrapping, by varying the delay Δt between the prepulse and the measurement pulse. Data illustrative for the method, taken on a contact with transmissions {0.91, 0.62, 0.15}, are shown Fig. 11: in a flux region exhibiting poisoning, the left panel shows $P_{sw}(s)$ for a short and a long delay Δt, and the right one the complete dependence of P_{sw} on Δt at a bias value $s = 0.826$, for which $P^0_{sw} \approx 1$ and $P^1_{sw} \approx 0$. The data are well fitted with an exponential dependence $P_{sw}(\Delta t) = P_\infty + (P_0 - P_\infty)\exp(-\Delta t/T_1)$. One can then extract the initial poisoning just after the prepulse $p_0 = 1 - P_0$, the asymptotic value at long times $p_\infty = 1 - P_\infty$, and the relaxation time T_1.

As discussed in the Letter, the dynamics of quasiparticle poisoning is strongly phase dependent. Measuring this phase dependence is however not trivial, because during the pulse sequence shown in Fig. 8, δ is not constant: it takes a value close to φ during Δt, then reaches $\sim \varphi + \gamma\left(s^{JJ}_{sw}\right)$ during the measurement pulse ($\gamma\left(s^{JJ}_{sw}\right) \simeq 0.3\pi$). As shown below, relaxation is very fast when $\delta > 1.3\pi$, so that data taken at $\varphi > \pi$ are dominated by the relaxation at measurement.

To correctly measure the phase dependence of the relaxation, we have therefore elaborated a different protocol, shown in Fig. 12. We set the flux imposed by the external coil to a value φ_i such that p_0 is far from 0, and that the relaxation times at φ_i and at $\varphi_i + \gamma\left(s^{JJ}_{sw}\right)$ are long, so that relaxation during the measurement can be neglected. We first take a switching curve $P_{sw}(s)$ and fit it with a weighted sum of two shifted curves as in

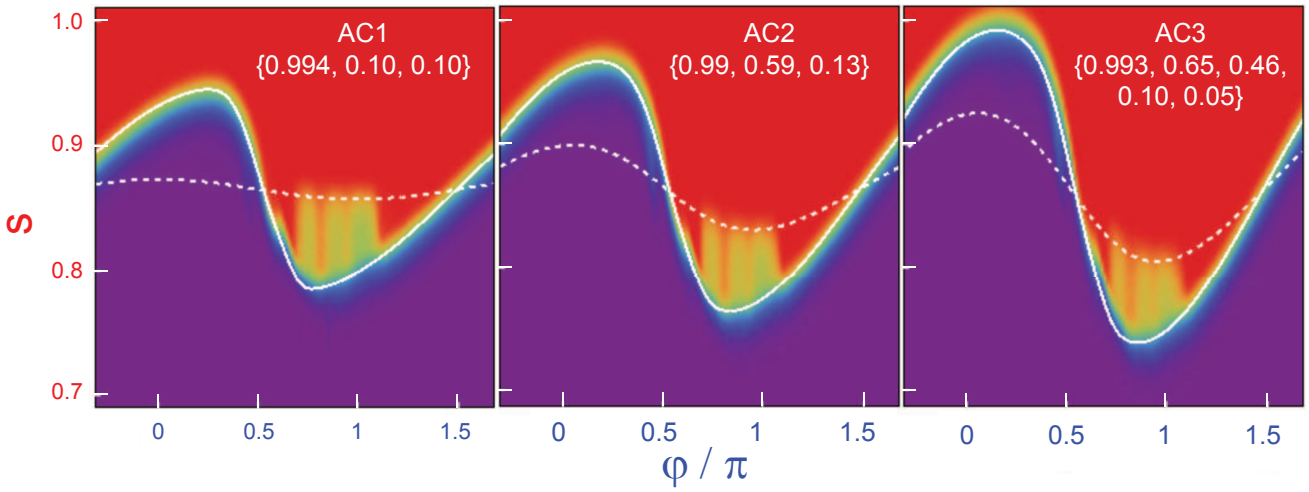

Figure 10: Color plot of the switching probability $P_{sw}(s,\varphi)$ using switching prepulses (see Fig. 8, with $\Delta t = 2\,\mu$s) for SQUIDs made with three different atomic contacts, each having one channel with a transmission close to 1: AC1, {0.994,0.10,0.10} (same data as in the Letter); AC2: {0.998,0.59,0.13} and AC3: {0.993,0.65,0.46,0.10,0.05}. The white curves correspond theoretically to $P_{sw} = 0.5$ for the pristine contact (solid line) and for the poisoned contact (dashed line).

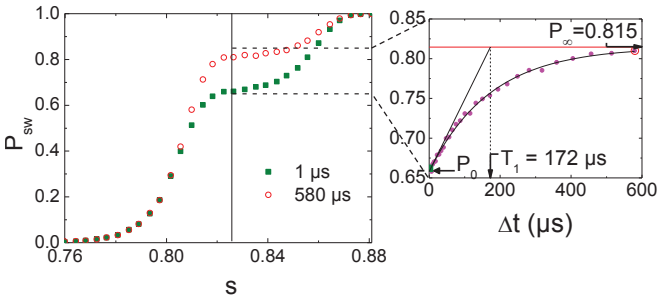

Figure 11: Left panel: Switching probability of contact {0.91, 0.62, 0.15} as a function of bias pulse height at fixed φ, for short ($\Delta t = 1\,\mu$s, green solid squares) and long ($\Delta t = 580\,\mu$s, red open circles) delay between the prepulse and the measurement pulse. Right panel: Dots: Evolution with Δt of the plateau height, measured at $s = 0.826$ (vertical line on the left panel). Solid line: exponential fit with $P_{sw}(\Delta t) = P_\infty + (P_0 - P_\infty)\exp(-\Delta t/T_1)$.

the inset of Fig. 9. We then fix a working point s_0 corresponding to the intermediate plateau, and determine the switching probabilities corresponding to the pristine contact $P^0_{sw}(s_0)$ and to the poisoned contact $P^1_{sw}(s_0)$. For all the data presented in the following, the working point was chosen such that $P^0_{sw}(s_0) = 1.00$ and $0.01 \leq P^1_{sw}(s_0) \leq 0.12$ (except for the data taken at higher temperatures, where the rounding of the curves becomes comparable to their width, and $P^1_{sw}(s_0)$ can be as high as 0.32). The probability p to be in an odd configuration is then inferred from

$$P_{sw}(s_0) = (1-p)P^0_{sw}(s_0) + pP^1_{sw}(s_0), \qquad (8)$$

which is slighlty more precise than the identification of p with $1 - P_{sw}(s_0)$. A measurement similar to that presented in Fig. 11 is then used to characterize the system at flux φ_i :

$$p(\varphi_i, \Delta t) = \mathcal{E}^{p_\infty(\varphi_i)}_{T_1(\varphi_i)}\left(p_0(\varphi_i), \Delta t\right) \qquad (9)$$

where we have introduced the function $\mathcal{E}^{p_\infty}_{T_1}(p_0, t)$ accounting for an exponential variation starting from p_0 and during time t, with characteristic time T_1 and asymptotic value p_∞ :

$$\mathcal{E}^{p_\infty}_{T_1}(p_0, t) \equiv p_\infty + (p_0 - p_\infty)\exp(-t/T_1). \qquad (10)$$

Using a dc flux pulse applied through the fast flux line between the prepulse and the measurement pulse, the flux phase is changed to a value φ_w for a time t_w (in practice, we leave a 1 µs delay between the prepulse and the flux pulse to let the system stabilize; we also leave a delay of t^0_w =15 µs between the flux pulse and the measurement pulse to get rid of ringing effects after the fast flux pulse). Since the bias current is 0 during this dc flux pulse, the phase across the atomic contact is then simply $\delta = \varphi_w$[29].

From the switching probability $P_{sw}\left(t_w + t^0_w\right)$ we calculate using Eq. (8) the probability $p\left(t_w + t^0_w\right)$ to be in an odd configuration after the complete sequence. We observe that $p\left(t_w + t^0_w\right)$ is not an exponential function of t_w. The reason is that this probability results from two exponential relaxations with different parameters, as illustrated at the bottom of Fig. 12. The initial value $p(0) = p_0(\varphi_i)$ results from the prepulse applied at phase flux φ_i (the function $p_0(\varphi_i)$ is discussed farther). Follows an exponential evolution at phase flux φ_w during t_w, leading to

$$p(t_w) = \mathcal{E}^{p_\infty(\varphi_w)}_{T_1(\varphi_w)}\left(p(0), t_w\right). \qquad (11)$$

During the last $t^0_w = 15\,\mu$s, the phase flux is φ_i, so that

$$p\left(t_w + t^0_w\right) = \mathcal{E}^{p_\infty(\varphi_i)}_{T_1(\varphi_i)}\left(p(t_w), t^0_w\right). \qquad (12)$$

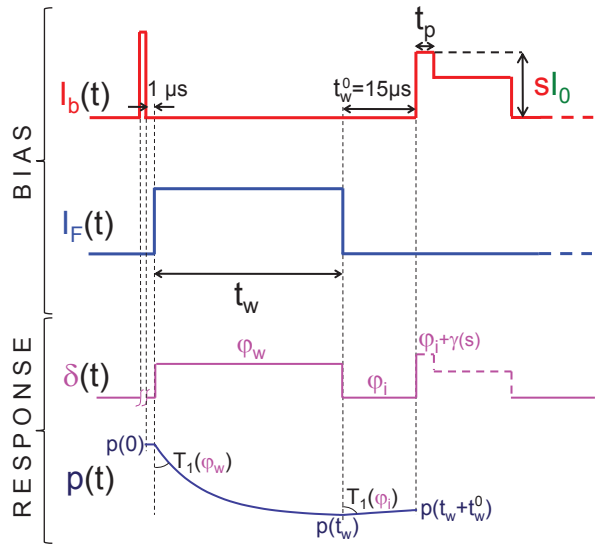

Figure 12: Pulse sequence used to measure the phase dependence of the relaxation process. The first line corresponds to the signal applied to the current bias, the second one to the fast flux line. The two last lines sketch the corresponding evolution of the phase δ across the atomic contact and of the poisoning probability $p(t)$. The prepulse causes systematic switching, and the "running away" of the phase is not represented. The dotted line in $\delta(t)$ during the measurement pulse indicates that either the SQUID switches and the phase runs away, or it does not switch and δ simply follows the bias current. The prepulse and the measurement pulse are always applied at the same flux phase φ_i. The probability $p(t)$ starts from $p(0)$ after the prepulse, a value that depends on the flux φ_i; a flux phase φ_w is then applied during a time t_w, and $p(t)$ relaxes exponentially with a time constant $T_1(\varphi_w)$ towards $p_\infty(\varphi_w)$, reaching $p(t_w)$. In the last step, the phase flux is restored to φ_i during $t_w^0 = 15\,\mu$s and $p(t)$ evolves with the time constant $T_1(\varphi_i)$ towards $p_\infty(\varphi_i)$, reaching finally $p(t_w + t_w^0)$, the actual value accessed by the measurement (the schematic corresponds to a situation where $p(t_w) < p_\infty(\varphi_i)$, hence $p(t)$ increases in the last step). In the time interval between the prepulse and the measurement pulse, the bias current I_b is zero, and the phase δ across the atomic contact is equal to the flux phase: $\delta = \varphi_w$ during t_w, then $\delta = \varphi_i$ during t_w^0.

Since the parameters $p(0)$, $T_1(\varphi_i)$ and $p_\infty(\varphi_i)$ have been determined in the first measurement without the flux pulse, Eq. (12) can be used to deduce $p(t_w)$ from $p(t_w + t_w^0)$. The function $p(t_w)$ is then an exponential, as expected, and its fit with Eq. (11) yields the asymptotic poisoning $p_\infty(\delta)$ and the relaxation time $T_1(\delta)$.

Using this more complex procedure that involves the fast flux line to apply dc flux pulses, the relaxation can be probed with the prepulse and the measuring pulse both acting always at the same flux. The initial value of the poisoning probability is therefore always the same, and the working point can be chosen such that relaxation during the measurement pulse plays no role (note that, as long as this last criterium is observed, $p_\infty(\delta)$ and $T_1(\delta)$ do not depend on the working point).

B. Temperature dependence

The functions $p_\infty(\delta)$ and $T_1(\delta)$ at various temperatures, are shown in Fig. 13 for contact AC1. Whereas $p_\infty(\delta)$ hardly changes, $T_1(\delta)$ drops rapidely with temperature, and relaxation is almost instantaneous above 220 mK.

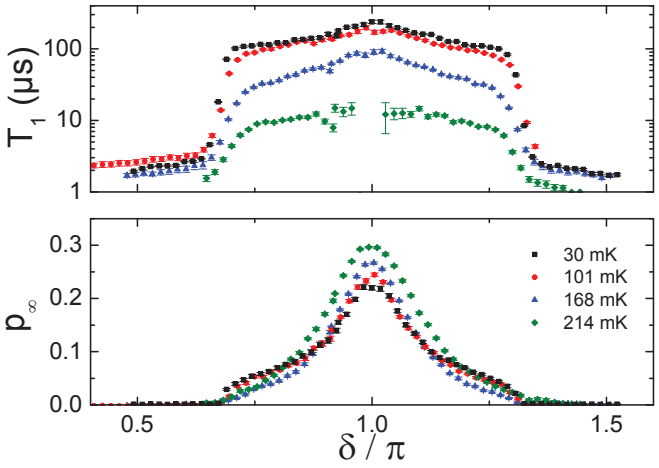

Figure 13: Relaxation time T_1 and asymptotic poisoning probability p_∞, as a function of the phase $\delta = \varphi_w$ applied during the dc flux pulse imposed for a time t_w between the prepulse and the measurement pulse. The data are taken on the atomic contact AC1 ($\{0.994, 0.10, 0.10\}$), and at four different temperatures T indicated in the figures.

C. Revisiting $P_{sw}(s, \varphi)$ data

Coming back to the results presented in the left panel of Fig. 10, the boundaries of the phase range in which poisoning occurs can be understood in the light of Fig. 13: the left boundary corresponds to the phase φ_L at which $T_1(\varphi_L)$ becomes comparable with $\Delta t = 2\,\mu$s, leading to significant relaxation in the time interval between the prepulse and the measurement pulse. The nature of the right boundary is different: it corresponds to the phase φ_R at which $T_1(\gamma(s) + \varphi_R)$ becomes comparable with $t_p = 1\,\mu$s (we recall that $\gamma(s)$ is the phase across the Josephson junction during the measurement pulse), leading to significant relaxation during the measurement pulse. In contrast with the left boundary, the position of the right one depends slightly on s through $\gamma(s)$, which explains that it is slightly tilted. Hence, in the simplest procedure where the flux is the same during the whole sequence, the effect of relaxation during the measurement pulse becomes predominent for $\varphi > \pi$, explaining why the intervals on which poinsoning is observed in Fig. 10 is not centered at π.

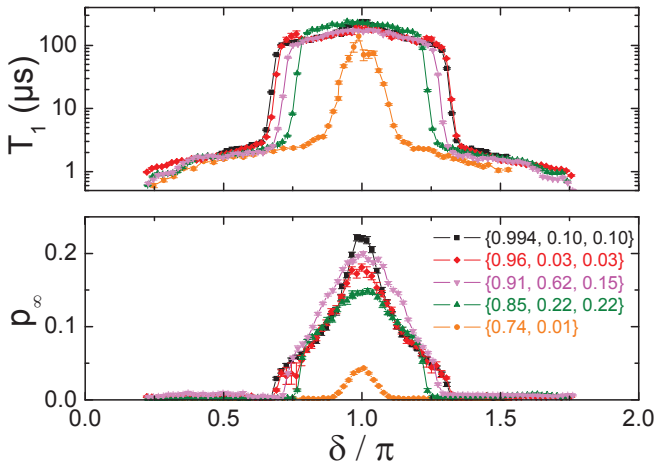

Figure 14: Relaxation time T_1 and asymptotic poisoning probability p_∞, measured at $T = 20\,\mathrm{mK}$, for five different atomic contacts with the shown transmissions.

D. Revisiting data without prepulses

The anomalous statistics of the time intervals between switching events mentioned above finds also an explanation. The data presented in Fig. 7 are taken without prepulse, so that if poisoning occurs after a measurement pulse, the system remains poisoned during a time T_1 in average, and switching is suppressed, giving rise to long "blind" periods. When the system unpoisons, switching occurs again, and, the probability to get poisoned again being rather small, several switching events occur in a row. When the repetition period T_r is increased, the probability to escape from a poisoned configuration before the next measurement increases. And since the switching rate is larger when the system is not poisoned, the average switching probability increases, as observed.

E. Raw data on several contacts

Similar data taken on a variety of atomic contacts are shown in Fig. 14. The phase interval in which poisoning occurs reduces when the transmission of the most transmitting channel diminishes. The same data are replotted as a function of E_A in Fig. 4 of the Letter.

F. Multiple poisoning

In a contact with more than one well transmitting channel, poisoning can affect several channels at once, as shown in Fig. 15 where the switching probability presents two intermediate plateaus. The first one near 0.5 corresponding to either one of the two first channels being poisoned (they have very similar transmissions), the second one at 0.95 to the situation in which both are.

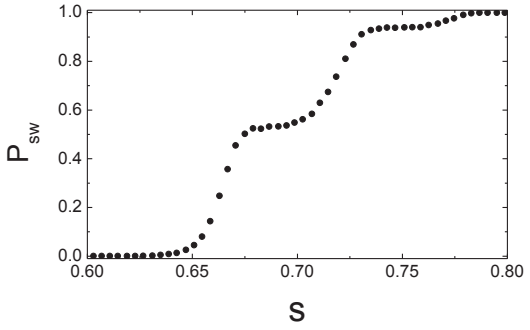

Figure 15: Measured switching probability as a function of s for a contact with two well transmitting channels: {0.96, 0.95, 0.60, 0.34, 0.30, 0.29, 0.27, 0.26, 0.24, 0.2}, taken at a flux within the poisoned region. The first plateau ($P_{sw} \simeq 0.55$) can be attributed to situations where one of the two channels with transmission ~ 0.95 is poisoned, while the second one corresponds to situations where both are poisoned.

G. Initial poisoning

We have measured the initial poisoning p_0 as a function of the phase δ across the atomic contact AC1 ({0.994,0.10,0.10}). The measurement protocol is shown in Fig. 16: the flux phase φ_{pp} applied till the end of the prepulse is varied, then the flux is reset to φ_i. Here again, the effect of relaxation at φ_i during the 15 µs between the end of the flux pulse and the measurement pulse has been corrected for. The result of the measurement is displayed in Fig. 17 (for the chosen value of φ_i, indicated with a dashed line, the relaxation before measurement is characterized by $T_1 = 167\,\mu\mathrm{s}$ and $p_\infty = 0.12$). This irregular pattern is responsible for the vertical stripes in the data shown in Fig. 10. Similar patterns, with slight dependence on the duration of the prepulse and on the rate of decay of the current at the end of the prepulse, were found on the other contacts, but the influence of the different parameters could not be deconvolved from the data.

VII. QUASIPARTICLE POISONING ANTIDOTE

The experimental data indicate that when the phase δ across the atomic contact is driven far from π, the system quickly relaxes to the ground state. Based on this result, we have developed a procedure to get rid of trapped quasiparticles. The principle, illustrated in Fig. 18, is simply to sweep the flux phase over 2π, with a pair of symmetric "antidote" pulses with amplitude π each, hence insuring that whatever the starting phase, δ crosses 0 or 2π. Poisoning is cured by the antidote pulses, as shown in Fig. 19 where we compare relaxation curves with and without them at $\varphi_w = \pi$ for contact AC1 ({0.994,0.10,0.10}), the flux phase value where the poisoning probability was the highest. Whereas data taken as in Fig. 11 (right panel) show initial poisoning with a

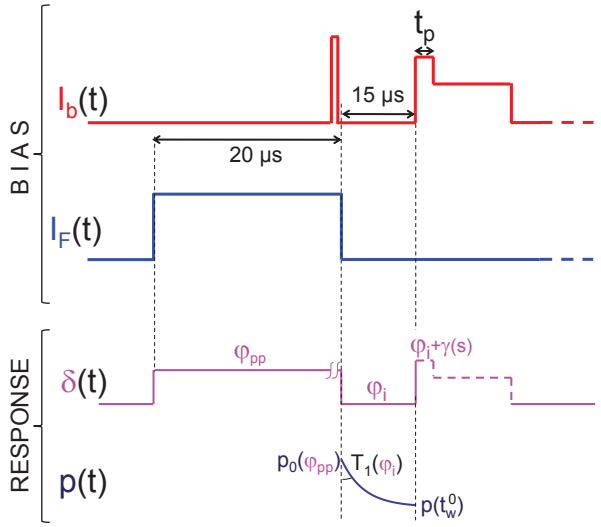

Figure 16: Pulse sequence used to measure the phase dependence of the initial poisoning probability p_0. The first line corresponds to the bias current, and the second one to the fast flux line. The third line sketches the evolution of the phase δ across the atomic contact, and the last one that of the poisoning probability. The quantity that is studied is the poisoning probability $p_0(\varphi_{pp})$ just after the prepulse, which depends on the phase flux φ_{pp} applied to the contact during the prepulse. Note that the measuring pulse gives access to $p(t_w^0)$, which includes relaxation at flux φ_i during the last $t_w^0 = 15\,\mu s$. This relaxation is taken into account to obtain $p_0(\varphi_{pp})$.

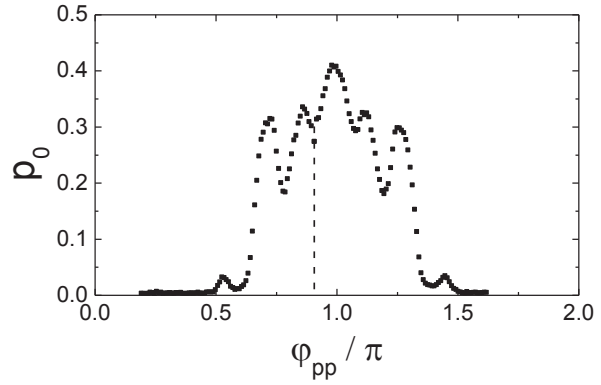

Figure 17: Initial poisoning p_0 as a function of the phase $\delta = \varphi_{pp}$ across the atomic contact AC2 at the end of the prepulse. The pulse sequence used to gather this data-set is shown in Fig. 16. The dashed line indicates the value of the phase δ across the atomic contact when only the dc flux φ_i is applied.

probability $p_0 = 0.37$, the poisoning probability extrapolates to 0 at $t_w = 0$ when antidote pulses are applied (Fig. 19, top curve), indicating that poisoning is absent just after the pulses. Remarkably, the subsequent evolution is identical in both situations, tending exponentially to $p = 0.23$ with a time constant $T_1 = 220\,\mu s$. The identical time constants and asymptotic poisoning probabil-

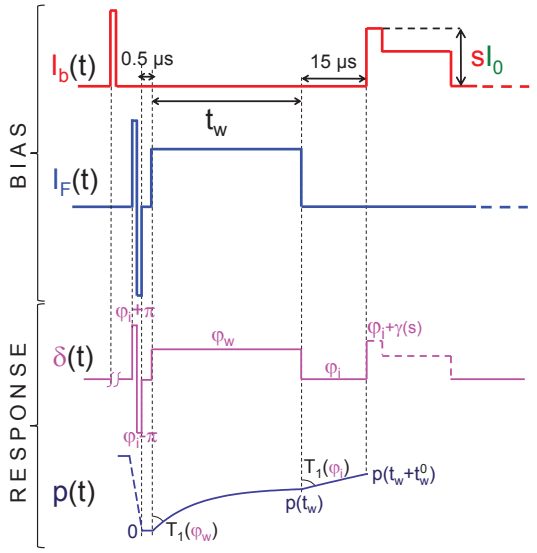

Figure 18: Pulse sequence used to measure the phase dependence of the relaxation process after the application of "antidote pulses". The first line corresponds to the current bias, and the second one to the fast flux line. The third line sketches the evolution of the phase δ across the atomic contact, and the last one that of the poisoning probability $p(t)$. The antidote pulses are pairs of dc flux pulses applied in both directions, with an amplitude corresponding to a phase excursion of π on the phase δ. Their total duration was 0.5 µs; they are applied 1.5 µs after the prepulse. During the pair of antidote pulses, the phase visits regions where a trapped quasiparticle escapes rapidly, and the poisoning probability decays to 0.

ity was checked on many atomic contacts. These data prove the robustness of the exponential behavior, and that poisoning associated with residual quasiparticles has the same effect whatever the initial configuration.

Antidote pulses were employed to record $P_{sw}(s,\varphi)$ on the SQUID with contact AC0, as shown in Fig. 20. We used the simplest current bias pulses, shown in Fig. 6, with antidote pulses applied on the flux line 1 µs before the measurement pulse. The region displaying poisoning in Fig. 7 has completely disappeared, and switching is regular for all values of the flux phase φ.

The procedure presented here allows to obtain with very high probability unpoisoned configurations, at least just after the antidote pulses. Nevertheless, attempts to induce transitions from state $|0\rangle$ to state $|2\rangle$ with microwaves applied on the fast flux line were unsuccessful in this experiment.

VIII. MECHANISM FOR INITIAL POISONING

The system always switches during the 0.1 µs-long prepulse, and a voltage of the order of $V = 0.1\,\mathrm{mV}$ develops across the atomic contact. The phase δ then varies rapidly, at the pace V/φ_0, and multiple Andreev reflec-

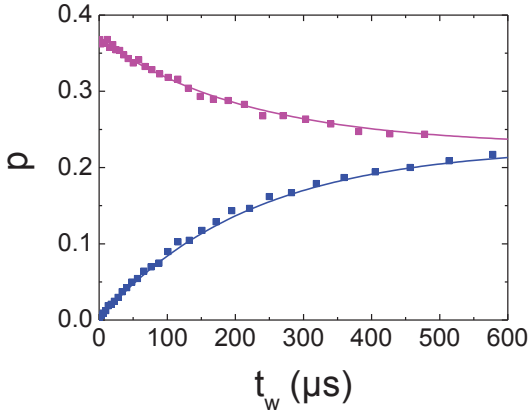

Figure 19: Symbols: Poisoning probability as a function of time t_w spent at phase π, for contact AC1 ({1,0.07,0.07}). Top curve is taken with the pulse sequence shown in Fig. 12, and shows frequent poisoning ($p(0) = 0.37$). Bottom curve has "antidote" flux pulses after the current prepulse (see Fig. 18), which suppress initial poisoning ($p(0) = 0$). Solid lines are exponential curves with identical time constants $T_1 = 220\,\mu s$ and asymptotic value $p = 0.23$.

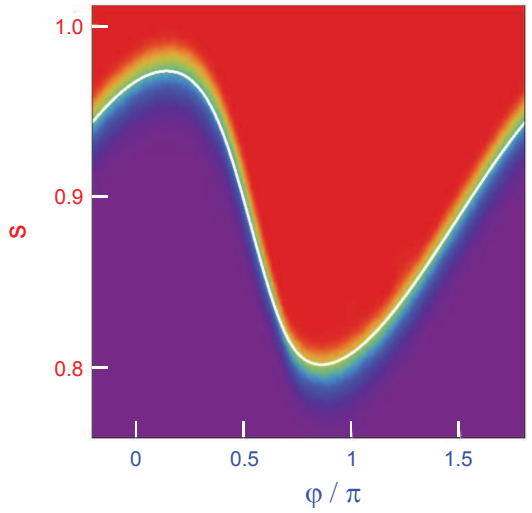

Figure 20: Color plot of the switching probability $P_{sw}(s,\varphi)$ using an antidote flux pulse 1 μs before the measurement pulse, and without prepulse, for the SQUID with contact AC0 with transmissions {0.95,0.45,0.10}. The color scale is the same as for Fig. 7. The white curve show the lines corresponding theoretically to $P_{sw} = 0.5$ for the full contact. This plot is to be compared with Fig. 7.

tions carry a current across the atomic contact, which creates quasiparticles on both sides of the contact[30]. For a contact of unit transmission, two quasiparticles are being created for each turn of the phase. The resulting number of quasiparticles is therefore $2 \times 0.1\,\mu s \times 0.1\,mV \times 2e/h \simeq 10^4$. When the bias current is reset to zero, the phase stops in a local minimum of the global potential, and the configuration of the Andreev levels freezes. The experiment indicates that after this step, the population of the Andreev states generally does not correspond to the equilibrium situation: there is a poisoning probability p_0 from which relaxation is subsequently observed. The exact process of poisoning after switching is not understood presently. One can however qualitatively grasp the mechanisms that can be relevant using the picture of the "Andreev elevator" that describes transport in the finite voltage state, at least for small voltages[30]: the phase varies linearly in time and the Andreev levels, in the semiconductor representation, coincide periodically with the gap edges of the continuum (when $\delta = 2n\pi$), loading the lower level with a quasiparticle at the lower continuum, and unloading it in the upper one. The quasiparticle is sometimes transferred from the lower level to the upper one by Landau-Zener tunneling. In this scenario, the system is always in an even configuration. However, many quasiparticles are created in the continuum, and the "loading" (or "unloading") process can fail, leading to a situation where, after passing $\delta = 2n\pi$, the lowest state is unoccupied while the upper one has emptied (or *vice versa*), leading to an odd configuration. If the system returns to the zero voltage state at this stage, the system stays trapped in the odd configuration. The oscillating structure for $p_0(\varphi_{pp})$ in Fig. 17 suggests that interferences during the phase dynamics may also play a role. Further work is clearly needed to clarify this phenomenon.

IX. MODEL FOR POISONING DYNAMICS

We now discuss with the help of Fig. 21, the details of the model presented in Fig. 4 of the Letter. Quasiparticles can jump between the Andreev states and quasiparticle states in the continuum. The processes are in

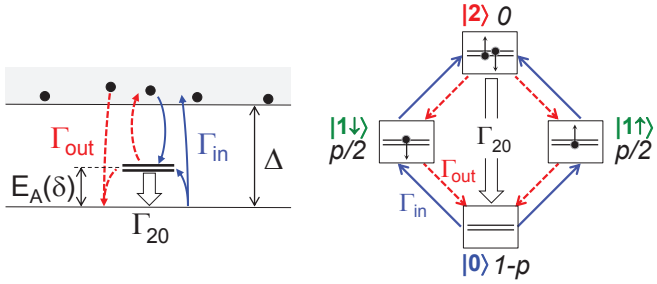

Figure 21: Model for the dynamics of the population of the Andreev configurations. *Left*: in the excitation representation. *Right*: in the configurations space, where the probability of the 4 configurations are given in italic. Quasiparticles can jump in and out the Andreev levels at rates Γ_{in} and Γ_{out}. If both levels of the Andreev doublet are occupied, the system can decay directly to the ground state (rate Γ_{20}).

principle rather slow because they either require energy absorption (rate Γ_{out}), or the presence of quasiparticles in the continuum (rate Γ_{in}). Because the state with a double excitation is never observed, we assume that the

relaxation rate Γ_{20} to the ground state is much larger than $\Gamma_{\rm in}$ and $\Gamma_{\rm out}$. This hypothesis is discussed in Appendix B.

The master equation for the populations of the ground state $|0\rangle$, $1-p$, and of the odd configurations $|1\uparrow\rangle$ and $|1\downarrow\rangle$, $p/2$ each, is (see right hand side of Fig. 21):

$$\frac{\mathrm{d}\,(1-p)}{\mathrm{d}t} = -2\,(1-p)\;\Gamma_{\rm in} + p\,(\Gamma_{\rm out}+\Gamma_{\rm in}), \qquad (13)$$

the term $+p\Gamma_{\rm in}$ corresponding to transitions from the odd configurations through the excited state $|2\rangle$ which relaxes very fast to the ground state. Assuming that $\Gamma_{\rm in}$ and $\Gamma_{\rm out}$ are time-independent, which is necessary to obtain the observed exponential dependence of $p(t)$, one gets equation (2) of the Letter. The assumption that $\Gamma_{\rm in}$, which is proportional to the quasiparticle density, is constant, means that quasiparticles created in the voltage state after switching have disappeared at the time scales probed by relaxation experiments. Experiments with a succession of several prepulses indicate that this is the case. One possibility is that they have already recombined. In the next paragraph, we argue that they have probably already diffuse away.

To evaluate the decay of the density n_{qp} of quasiparticles occurring due to just diffusion, we start from the number of quasiparticles created during the prepulse, 10^4, as evaluated at the beginning of Section VIII. Within the duration of the prepulse, they spread over $\sim \sqrt{D_{qp}\times 0.1\,\mu\mathrm{s}} > \sqrt{D_N\times 0.1\,\mu\mathrm{s}} \simeq 50\,\mu\mathrm{m}$ (with $D_{qp} = D_N/\left(1-(\Delta/E)^2\right)$ the diffusion constant for quasiparticles of energy E in the superconducting state[31], D_N the value in the normal state), *i.e.* over the whole area of SQUID (see Fig. 3(c)). The density at the end of the prepulse is therefore $n_{qp}^0 \approx 100\,\mu\mathrm{m}^{-3}$. Diffusion is then one-dimensional because it is limited by the 3 thin connections (inductive lines), and a rough estimate (using again the diffusion constant D_N instead of D_{qp}) indicates that the density decays within a few microseconds below $10\,\mu\mathrm{m}^{-3}$, which is the typical background value found for Al films at low temperatures in Refs. [32,33]. The quasiparticles created by the prepulse can therefore be neglected when describing the dynamics of poisoning relaxation.

X. QUASIPARTICLE TRAPS

Let us note that in previous experiments with atomic contacts in SQUIDs[9,30] we didn't observe poisoning. In these works, the superconducting loop was directly connected to very large normal metal electrodes, which acted as efficient quasiparticle traps. In the present case, our SQUID is contacted through very narrow and thin superconducting lines, and clearly the small pieces of gold placed in direct contact with the present SQUID body didn't act as efficient quasiparticle traps. In fact, a normal metal electrode can only act as a trap if it is so large that the diffusion time of a quasiparticle through it exceeds the relaxation time of its energy.

On the other hand, the decoupling from dissipative parts of the circuit is an important requirement[34] in order to explore the physics of the Andreev qubit[35–37], and the use of normal metal traps is probably not advisable. As a consequence, there would always be some quasiparticles ready to get trapped in the Andreev bound states. One method to get rid of them is to use the "antidote pulses" described in Section VII. Another method is to have connecting wires with a lower gap than the SQUID. We checked experimentally, using bilayers of Al and Cu, that it allows to get rid of poisoning.

Appendix A: SQUID potentials

The SQUID potential is given by Eq. (6). If transitions between configurations are slow compared to the plasma frequency, which is the characteristic timescale for the dynamics in $U(\gamma)$, the escape rate is determined by the potential corresponding to the instantaneous configuration[38]. As an example, we plot in Fig. 22 the three potentials for a contact with a single channel with transmission 0.99, at $\varphi/\pi = 0.9$, and for $s = 0$ and $s = 0.87$. The plot at $s = 0$ matters for the evaluation of the transmission rates during Δt, whereas the plot at $s = 0.87$ aims at illustrating why the switching rates are very different in the ground state of the channel and in the odd configurations. The energies $E_J = 1.14\,\mathrm{meV}$ and $\Delta = 0.193\,\mathrm{meV}$ correspond to the parameters of the Josephson junction of the experiment. The distance in energy between the potentials is the smallest when $\delta = \pi$, *i.e.* $\gamma = \pi - \varphi = 0.1\pi$. We also indicate the ground state energy in each potential, as obtained from semi-classical calculations. The quantum fluctutations of γ (and hence of δ) are of the order of 0.1π. When the flux phase φ is different from 0 and π, as in the example of Fig. 22, the three potentials do not have their minima at the same value of γ, an effect that is expected to modify the transition rates between configurations[11].

At $s = 0.87$, the barrier heights are strongly reduced. The barrier is the smallest in the ground state, and switching occurs only if the system is in the ground state, and not in the odd configuration, as is the case in Fig. 10 for $\varphi/\pi = 0.9$ between the dotted line and the solid line.

Appendix B: relaxation between Andreev states

The excited doublet $|2\rangle$ is never observed in our experiments. We have attributed this fact to a large value of the relaxation rate Γ_{20} to the ground state. Two contributions to this rate can be evaluated. The first one is the rate $\Gamma_{20}^{\rm em}$ of the process in which a photon is emitted into

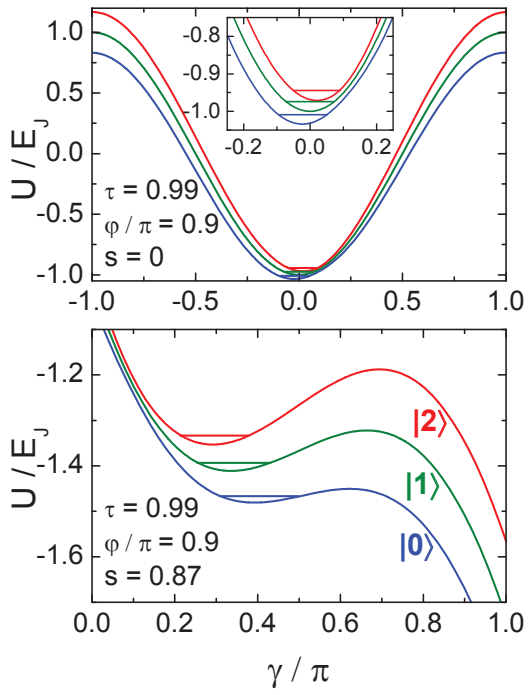

Figure 22: Potentials of a SQUID with a single channel atomic contact with transmission $\tau = 0.99$, at $\varphi/\pi = 0.9$ and $s = 0$ (top panel) or $s = 0.87$ (bottom panel). The three curves correspond, from top to bottom, to the atomic contact in the ground state $|0\rangle$ (blue), in the odd configuration $|1\rangle$ (green), and in the excited state $|2\rangle$ (red). Horizontal lines indicate the energy of the first level $\frac{1}{2}\hbar\omega_p$ in each potential, with the plasma frequency $\omega_p/2\pi$ calculated semi-classically (at $s = 0$, $\omega_p^{|0\rangle}/2\pi = 12.3\,\mathrm{GHz}$, $\omega_p^{|1\rangle}/2\pi = 14.1\,\mathrm{GHz}$, $\omega_p^{|2\rangle}/2\pi = 14.8\,\mathrm{GHz}$; at $s = 0.87$, $\omega_p^{|0\rangle}/2\pi = 7.9\,\mathrm{GHz}$; $\omega_p^{|1\rangle}/2\pi = 9.7\,\mathrm{GHz}$; $\omega_p^{|2\rangle}/2\pi = 10.9\,\mathrm{GHz}$). The energy scale is $E_J = 1.14\,\mathrm{meV} \approx 13\,\mathrm{k_B K}$.

the electromagnetic environment of the atomic contact[34]:

$$\Gamma_{20}^{\mathrm{em}} = \frac{\pi\Delta}{\hbar}\frac{\mathrm{Re}\left[Z_t\left(2E_A/\hbar\right)\right]}{h/e^2}\frac{1-\tau}{\left(E_A/\Delta\right)^3}\left[\tau\,\sin^2\left(\frac{\delta}{2}\right)\right]^2 \tag{14}$$

Note that this equation actually differs by the last factor from the one in Refs. [34], because we have used to describe the Andreev system the hamiltonian proposed in Ref. [36] instead of the one introduced in Ref. [41] which does not enforces charge neutrality. For the actual circuit design (Fig. 3), the environment impedance Z_t is:

$$Z_t^{-1}(\omega) = jC_{JJ}\omega + \frac{1}{jL_{JJ}\omega} + \frac{1}{jL\omega + \frac{1}{\left(r+\frac{1}{jC\omega}\right)^{-1}+R_b^{-1}}}, \tag{15}$$

where $L_{JJ} = \varphi_0/I_0$, C_{JJ} are the Josephson junction inductance and capacitance, respectively. The eigenmodes of the two LC circuits, at $1/(2\pi\sqrt{LC}) \simeq 0.5\,\mathrm{GHz}$ and $1/(2\pi\sqrt{L_{JJ}C_{JJ}}) \simeq 14.5\,\mathrm{GHz}$, couple to give two peaks near 0.4 GHz and 17 GHz; between 0.5 GHz and 15.3 GHz and above 16.6 GHz, the impedance $\mathrm{Re}Z_t$ is smaller than $1\,\Omega$. The resulting rate $\Gamma_{20}^{\mathrm{em}}$, shown with solid lines in Fig. 23, exceeds 1 MHz near $\delta = \pi$ when the transmission is large enough. Note that these estimations depends crucially on the value of the losses in the capacitor, which are modelled by $r = 0.5\,\Omega$, a value determined from low-frequency (0.5 GHz) measurements. When the Andreev frequency $2E_A/h$ is large, the losses could easily be very different, and the rate much larger.

The second contribution to Γ_{20} is the rate $\Gamma_{20}^{\mathrm{ph}}$ of the process in which a phonon is emitted. An upper bound to this rate[40] has been calculated in Refs. [37,41] in the limit $E_A \ll \Delta$:

$$\Gamma_{20}^{\mathrm{ph}} \simeq (1-\tau)\,\frac{\Delta}{E_A}\tau_{ph}^{-1}(E_A), \tag{16}$$

with $\tau_{ph}^{-1}(E) = \kappa_{ph}\,E^3$ the bulk electron-phonon relaxation rate at energy E. Experiments[42–44] on similar Al films give $\kappa_{ph} \simeq 3\,\mu\mathrm{s}^{-1}\mathrm{K}^{-3}$. The corresponding predictions are shown with dashed lines in Fig. 23 for transmissions 0.80, 0.95 and 0.995. Only for $\tau \leq 0.80$ does the rate $\Gamma_{20}^{\mathrm{ph}}$ exceed 1 MHz for phases around π. Therefore, the large value of Γ_{20} in the phase interval where poisoning is observed (at the MHz scale, which is the upper bound to the measured values of $\Gamma_{in,out}$, see Fig. 4 of Letter) can be attributed to losses in the electromagnetic environment of the atomic contact and, to a lesser amount, to phonon emission.

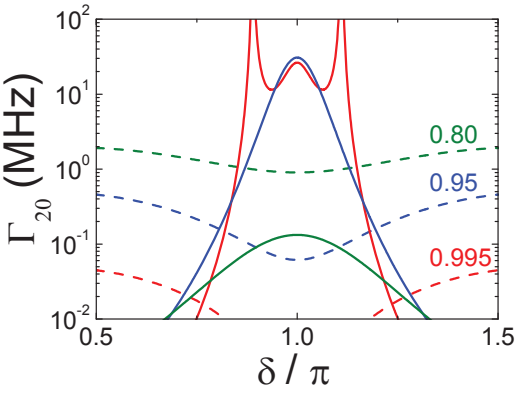

Figure 23: Calculated prediction for the relaxation rate Γ_{20} from the excited singlet, for transmissions $\tau = 0.8$, 0.95 and 0.995. Two contributions are plotted: rate for photon emission into the electronic environment $\Gamma_{20}^{\mathrm{em}}$ (solid lines) and upper bound[40] for the phonon emission rate $\Gamma_{20}^{\mathrm{ph}}$ (dashed lines). For $\tau = 0.995$, three peaks are visible in $\Gamma_{20}^{\mathrm{em}}$, corresponding to the Andreev frequency $2E_A/h$ approaching the low frequency mode of the electromagnetic environment at 0.4 GHz (central, broad peak) or coinciding with the high frequency mode at 17 GHz (lateral, sharp peaks). For smaller transmissions, only the effect of the high frequency mode is visible.

Given the values calculated for Γ_{20}, one could expect sharp spectroscopic signatures of the transition $|0\rangle \to |2\rangle$ when microwaves are applied. However, no clear trace of this effect could be found in the experiment. This could be due to imperfections in the implementation of

the microwave environment of the SQUID, or to additional relaxation channels.

[1] Present address: Institute of Physics, Polish Academy of Sciences, Al. Lotników 32/46, 02-668 Warszawa, Poland.
[2] M. Tinkham, *Introduction to Superconductivity* (McGraw-Hill, New York, 1975).
[3] S. Datta and P. F. Bagwell, Superlattices and Microstructures, 25, no 5-6, 1233 (1999)
[4] J. Michelsen, V. S. Shumeiko and G. Wendin, Phys. Rev. B **77**, 184506 (2008).
[5] Nikolai M. Chtchelkatchev and Yu.V. Nazarov, Phys. Rev. Lett. **90**, 226806 (2003).
[6] E. Vecino, A. Martín-Rodero, and A. Levy Yeyati, Phys. Rev. B **68**, 035105 (2003).
[7] Tobias Meng, Serge Florens and Pascal Simon, Phys. Rev. B **79**, 224521 (2009).
[8] Martin Chauvin, Ph. D. Thesis, Université Paris 6 (2005). Available (in English) from http:/tel.ccsd.cnrs.fr; B. Huard, Ann. Phys. Fr. 31, N° 4-5 (2006).
[9] M. L. Della Rocca, M. Chauvin, B. Huard, H. Pothier, D. Esteve, and C. Urbina, Phys. Rev. Lett. **99**, 127005 (2007).
[10] N.E. Booth, Appl. Phys. Lett. **50**, 293 (1987).
[11] Q. Le Masne, PhD thesis, Université Paris 6 (2009) (in English, available on the website tel.ccsd.cnrs.fr).
[12] Small indium pads placed on the contact pads and on the ground plane allow for more reliable contacts.
[13] H. Le Sueur and P. Joyez, Rev. Sci. Instrum. **77**,115102 (2006).
[14] T. Greibe, T. Bauch, C. Wilson, and P. Delsing, J. Physics: Conf. Ser. **150**, 052063 (2009).
[15] D. Averin and A. Bardas, Phys. Rev. Lett. **75**, 1831 (1995).
[16] E. N. Bratus', V. Shumeiko, and G. Wendin, Phys. Rev. Lett. **74**, 2110 (1995).
[17] J.C. Cuevas, A. Martin-Rodero, and A. L. Yeyati, Phys. Rev. B **54**, 7366 (1996).
[18] T.M. Klapwijk, G.E. Blonder and M. Tinkham, Physica B **109&110**, 1657 (1982).
[19] E. Scheer, P. Joyez, D. Esteve, C. Urbina, and M. H. Devoret, Phys. Rev. Lett. **78**, 3535 (1997).
[20] N. Agrait, A. Levy Yeyati, and J. van Ruitenbeek, Phys. Rep. **377**, 81 (2003).
[21] Robert M. Dickson, Andrew B. Cubitt, Roger Y. Tsien and W. E. Moerner, Nature **388**, 355 (1997).
[22] Sándor Volkán-Kacsó, Pavel A. Frantsuzov, Boldizsár Jankó, Nano Letters **10**, 2761 (2010), and references therein.
[23] W.C. Stewart, Appl. Phys. Lett. **12**, 277 (1968).
[24] D.E. McCumber, J. Appl. Phys. **39**, 3113 (1968).
[25] Vinay Ambegaokar and B. I. Halperin, Phys. Rev. Lett. **22**, 1364 (1969).
[26] P. Hänggi, P. Talkner, and M. Borkovec, Rev. Mod. Phys. **62**, 251 (1990).
[27] M. H. Devoret, D. Esteve, C. Urbina, J. Martinis, A. Cleland, and J. Clarke, in *Quantum Tunneling in Condensed Media* (Elsevier, 1992), p. 313.
[28] The elevated switching temperature can be attributed partly to spurious noise, partly to the proximity to the cross-over temperature for which quantum tunneling becomes equally important.
[29] The phase drop $\arcsin\left(I\left(\delta\right)/I_0\right)$ across the Josephson junction, at most of the order of 0.03π, is neglected.
[30] M. Chauvin, P. vom Stein, D. Esteve, C. Urbina, J. C. Cuevas, and A. Levy Yeyati, Phys. Rev. Lett. **99**, 067008 (2007).
[31] In contrast with what is often stated, Usadel theory indicates that quasiparticles in superconductors diffuse much faster than in the normal state. See for example Jan Petter Morten, Arne Brataas, and Wolfgang Belzig, Phys. Rev. B **70**, 212508 (2004).
[32] M. D. Shaw, R. M. Lutchyn, P. Delsing, and P. M. Echternach, Phys. Rev. B **78**, 024503 (2008).
[33] John M. Martinis, M. Ansmann, and J. Aumentado, Phys. Rev. Lett. **103**, 097002 (2009).
[34] M. A. Despósito and A. Levy Yeyati, Phys. Rev. B **64**, 140511(R) (2001).
[35] J. Lantz, V. S. Shumeiko, E. Bratus, and G. Wendin, Physica C:Superconductivity **368**, 315 (2002).
[36] A. Zazunov, V. S. Shumeiko, E. N. Bratus', J. Lantz, and G. Wendin, Phys. Rev. Lett. **90**, 087003 (2003).
[37] A. Zazunov, V. S. Shumeiko, G. Wendin, and E. N. Bratus', Phys. Rev. B **71**, 214505 (2005).
[38] In the opposite limit, the effective potential is build from the average current, see Refs. 11,39.
[39] H. Fritz and J. Ankerhold, Phys. Rev. B **80**, 064502 (2009).
[40] The rate is reduced due to the confinment of the bridge where the atomic contact is formed, see Ref. 37.
[41] D.A. Ivanov and M.V. Feigel'man, JETP Letters **68**, 890 (1998).
[42] P. Santhanam and D. E. Prober, Phys. Rev. B **29**, 3733 (1984).
[43] Anne Anthore, Ph. D. Thesis, Université Paris 6 (2003). Available (in English) from http:/tel.ccsd.cnrs.fr
[44] The definition of the electron-phonon scattering rate $\tau_{ph}^{-1}\left(E\right)$ in Ref. 37 is related to the characteric rate τ_0^{-1} introduced in Ref. 45 by $\tau_0^{-1}=\tau_{ph}^{-1}\left(k_BT_c\right)$. It differs by a factor $6\xi\left(3\right)\approx 7$ from the inelastic rate $\tau_{ep}^{-1}\left(T\right)$ due to electron-phonon processes in Ref. 42, which is an average on the scattering rates of electrons with energies in the width of the Fermi distribution[46]. Assuming that the matrix element for emission of phonons with energy ε is $\kappa_{ph}\varepsilon^2$, one has $\tau_{ph}^{-1}=\kappa_{ph}E^3$ and $\tau_{ep}^{-1}=6\xi\left(3\right)\tau_{ph}^{-1}$.
[45] S. B. Kaplan, C. C. Chi, D. N. Langenberg, J. J. Chang, S. Jafarey, and D. J. Scalapino, Phys. Rev. B **14**, 4854 (1976).
[46] F. Pierre, Ann. Phys. (Paris) **26**, No. 4 (2001).